Philosophical Magazine

ISSN: 1478-6435 (Print) 1478-6443 (Online) Journal homepage: http://www.tandfonline.com/loi/tphm20

New polytypes of LPSO structures in an Mg–Co–Y alloy

Q. Q. Jin, X. H. Shao, X. B. Hu, Z. Z. Peng & X. L. Ma

To cite this article: Q. Q. Jin, X. H. Shao, X. B. Hu, Z. Z. Peng & X. L. Ma (2017) New polytypes of LPSO structures in an Mg–Co–Y alloy, Philosophical Magazine, 97:1, 1-16, DOI: 10.1080/14786435.2016.1241909

To link to this article: https://doi.org/10.1080/14786435.2016.1241909

PHILOSOPHICAL MAGAZINE, 2017
VOL. 97, NO. 1, 1–16
http://dx.doi.org/10.1080/14786435.2016.1241909

Taylor & Francis
Taylor & Francis Group

New polytypes of LPSO structures in an Mg–Co–Y alloy

Q. Q. Jin[a,b†], X. H. Shao[a†], X. B. Hu[a#], Z. Z. Peng[a,b] and X. L. Ma[a]

[a]Shenyang National Laboratory for Materials Science, Institute of Metal Research, Chinese Academy of Sciences, Shenyang, China; [b]School of Materials Science and Engineering, University of Science and Technology of China, Hefei, China

ABSTRACT

The magnesium alloys containing long-period stacking ordered (LPSO) structures exhibit excellent mechanical properties. Each LPSO structure is known to contain either AB′C′A or AB′C building block and feature its own stacking sequences. By atomic-scale high-angle annular dark field scanning transmission electron microscopy, we find the co-existence of AB′C′A and AB′C building block in a single LPSO structure of the as-cast $Mg_{92}Co_2Y_6$ (at.%) alloy, leading to the formation of six new polytypes of the LPSO structures determined as 29H, 51R, 60H, 72R, 102R and 192R. The lattice parameter of each LPSO structure is derived as $a_{\mathrm{LPSO}} = a_{\mathrm{Mg}} = 0.321\mathrm{nm}$ and $c_{\mathrm{LPSO}} = \frac{1}{2}n \times c_{\mathrm{Mg}}$ (n presents the number of basal layers in a unit cell). The stacking sequences and the space groups of these newly identified LPSO structures are proposed based on the electron diffraction and atomic-scale aberration-corrected high-resolution images. A random distribution of Co/Y elements in the basal planes of AB′C′A and AB′C structural units is also observed and discussed.

ARTICLE HISTORY
Received 26 February 2016
Accepted 23 September 2016

KEYWORDS
Magnesium alloys; long-period stacking ordered (LPSO) structure; scanning transmission electron microscopy; electron diffraction

1. Introduction

The dilute magnesium alloys containing small amount of Zn and rare-earth (RE) elements have received considerable attention due to their excellent mechanical properties [1–3] and superior properties of corrosion resistance [4,5]. For example, The $Mg_{97}Zn_1Y_2$ (at.%) alloy developed by rapid solidification powder metallurgy process exhibits a maximum tensile yield strength exceeding 600 MPa with elongation of 5% at room temperature [1,2]. Various as-cast $Mg_{97}TM_1RE_2$ (TM = Zn, Ni, Cu; RE = rare earth) alloys [6–8] are also confirmed to exhibit tensile yield strength higher than 297 MPa after conventional hot-extrusion process. It is believed that the superior mechanical properties result from the presence of the long-period stacking ordered (LPSO) structures which is harder than Mg matrix, as well as grain refinement [1–3].

An LPSO structure features either a rhombohedral (R) or a hexagonal (H) Bravais lattice, depending on the stacking sequence of the close-packed atomic layers. It is usually named

CONTACT X. L. Ma xlma@imr.ac.cn

†Authors contributed equally in this work.

#Current Address: Nanostructures Research Laboratory, Japan Fine Ceramics Center, Nagoya 456–8587, Japan.

by the Ramsdell symbols. For example, the 18R LPSO phase exhibits a rhombohedral (R) Bravais lattice in which there are 18 close-packed atomic layers in the unit cell [9,10]. The structural characteristics of an LPSO structure, including the feature of stacking sequences and the ordering of M/RE elements in the basal plane, vary with the history of metallurgical and subsequent thermal processes to the alloys [6–18]. The metal elements M in Mg–M–RE systems play an important role in affecting the stacking sequence of the LPSO structures. The 10H, 18R, 14H and 24R LPSO structures are characterised by the AB′C′A building blocks [6–13]. In contrast, the 15R, 12H and 21R LPSO structures feature the building blocks of AB′C [14]. The M and/or RE atoms are rich in the B′C′ and B′ layers of the AB′C′A and AB′C building blocks, respectively. The elements, composition and heat treatment process are also known to determine the ordering of M/RE elements in the basal plane. It is reported that the Al and Gd atoms are ordered in the 18R and 14H structures in the Mg–Al–Gd alloys [11,12,15], while the Ni/Y elements are completely disordered in the basal plane of LPSO structures in Mg–Ni–Y alloys [8,16]. It is also know that the degree of the Zn/Y ordering in the basal planes of LPSO structures increases with the variety of the compositions from $Mg_{97}Zn_1Y_2$ [3,17], $Mg_{85}Zn_6Y_9$, to $Mg_{75}Zn_{10}Y_{15}$ [17]. Moreover, the Zn_6Y_8 cluster in the 10H structure of the as-cast $Mg_{75}Zn_{10}Y_{15}$ (at.%) alloy becomes more ordered after the alloy is annealed at 773 K for 24 h [18].

Based on the above experimental observations, we propose that the AB′C′A and AB′C building blocks or/and chemical ordering coexist in an LPSO structure if the composition of an alloy is appropriately designated. In this work, we focus on the LPSO structures in an $Mg_{92}Co_2Y_6$ (at.%) alloy. In addition to the previously reported 15R, 12H and 18R structures [14], we find several new polytypes of LPSO structures which are determined as 72R, 29H, 102R, 192R, 51R and 60H. Each of these new polytypes is composed of AB′C and AB′C′A building blocks, as clearly identified by the atomic-scale HAADF-STEM images.

2. Crystallography and notations of LPSO structures in the Mg–M–RE alloys

To determine the new LPSO structures, the crystallography of closely packed structures are applied [19,20]. Taken a monometallic system into account, the plane point group of a closely packed structure of a single atomic layer is $6mm$, while the plane point group of a multi-layered structure is $3m1$. The successive L stacking layers would introduce a stacking vector $\boldsymbol{t}$. In hexagonal coordinate, $\boldsymbol{a}$ and $\boldsymbol{b}$ denote hexagonal basic translational vectors within the layer and $\boldsymbol{c}$ is a vector perpendicular to $\boldsymbol{a}$ and $\boldsymbol{b}$. If $\boldsymbol{t} = \boldsymbol{c}$, the structure is hexagonal (H) structure, where the neighbour L layers are of same stacking sequence, as is shown in Figure 1(a). If $\mathbf{t} = \frac{\mathbf{a}}{3} + \frac{2\mathbf{b}}{3} + \frac{\mathbf{c}}{3}$, the structure is anti rhombohedral (R) structure, where the atoms in the 1st, L + 1st, $2L$ + 1st and $3L$ + 1st layers locate at position A, C, B and A (Figure 1(b)). If $\mathbf{t} = \frac{2\mathbf{a}}{3} + \frac{\mathbf{b}}{3} + \frac{\mathbf{c}}{3}$, the structure is positive rhombohedral (R) structure, where the atoms in the 1st, L + 1st, $2L$ + 1st and $3L$ + 1st layers locate at position A, B, C and A (Figure 1(c)). One unit cell of the rhombohedral structure thus consists of $3L$ layers. The minimum symmetry of these closely packed structures are $P3m1$ and $R3m$. Special symmetry operators, such as screw axis 2_1, inversion centre $\bar{1}$ and mirror plane $m_\perp$, may exist in the closely packed structures, as shown in Figure 1(d)–(g). The combination of these symmetry operations and the plane point group $3m1$ will result in new symmetry operations and space groups, as listed in Table 1. It should be noted that the selected-area electron diffraction (SAED) patterns of all the seven stacking ordered structures, as listed

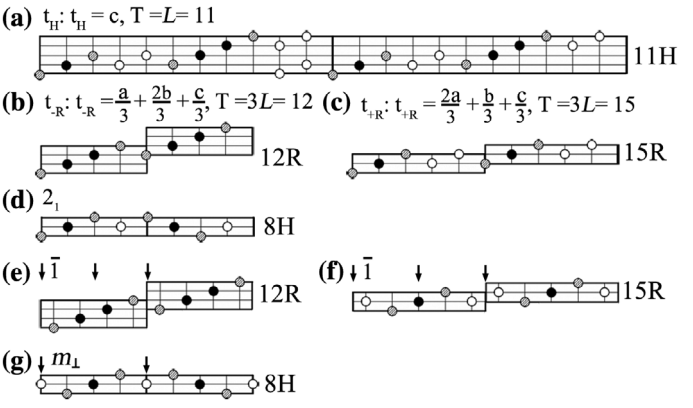

Figure 1. Structure models of 11H, 12R, 15R and 8H viewed along $[2\,\bar{1}\,\bar{1}\,0]_\alpha$ zone axis, showing the translation periodicity and symmetry operations $\bar{1}$, 2_1 and $m_\perp$ in close-packed structures.

Table 1. Relationship between extra symmetry operations, Bravias lattices and space groups of the stacking ordered structures.

Bravias Lattices	3	$\bar{3} = 3 + \bar{1}$	$6_3 = 2_1 + 3$	$\bar{6} = 3 + m_\perp$	$6_3/m$
Rhombohedral $\mathbf{t}_R$	*R*3*m*	*R*$\bar{3}$*m*			
Hexgonal $\mathbf{t}_H$	*P*3*m*1	*P*$\bar{3}$*m*1	*P*6$_3$*mc*	*P*$\bar{6}$*m*2	*P*6$_3$/*mmc*

Table 2. Reflection conditions of $\langle 0\,0\,0\,l\rangle$, $\langle 1\,\bar{1}\,0\,l\rangle$ and $\langle 1\,1\,\bar{2}\,l\rangle$ diffraction arrays of stacking ordered structures.

Space groups	$\langle 0\,0\,0\,l\rangle$	$<1\,\bar{1}\,0\,l\rangle$	$\langle 1\,1\,\bar{2}\,l\rangle$
*P*3*m*1, *P*$\bar{3}$*m*1, *P*$\bar{6}$*m*2	$l = n$	$l = n$	$l = n$
*P*6$_3$*mc*, *P*6$_3$/*mmc*	$l = 2n$	$l = n$	$l = 2n$
*R*3*m*, *R*$\bar{3}$*m*	$l = 3n$	$l = 3n + 1$, or $3n - 1$	$l = 3n$

in Table 1, are the same when they are taken along the [0 0 0 1] zone axis. The remarkable differences are (0 0 0 *l*) and (0 $\bar{1}$ 1 *l*) array in [2 $\bar{1}$ $\bar{1}$ 0] zone axis, and (0 0 0 *l*) and (1 1 $\bar{2}$ 0) arrays in [0 1 $\bar{1}$ 0] zone axis. The reflection conditions of $\langle 0\,0\,0\,l\rangle$, $\langle 0\,\bar{1}\,1\,l\rangle$ and $\langle 1\,1\,\bar{2}\,l\rangle$ arrays are listed in Table 2 [21].

A number of schemes of notation are used to describe the polytypes of a crystal with layered structure such as CdI_2, PbO_2 and SiC [22]. These schemes are also used to express the LPSO structure in Mg–M–RE alloys [9,10,14], as labelled in Table 3. Usually, an LPSO structure in the Mg–M–RE alloys is named by one of the Ramsdell symbols, where the number indicates the layers in one unit cell and the letter denotes the Bravais lattice. In addition, there are three traditional ways to characterise the LPSO structures. The first is based on the stacking sequences [9,14]. For example, 15R structure can be expressed as 15R – AB′CBC BC′ACA CA′BAB. The second is on Jagodzinski notations [10]. The 15R structure is described as *hchhhhchhhhchhh*, where *h* means the local HCP environment and *c* indicates the local FCC environment. The third is on Zhdanov symbols [9,23]. The 15R is expressed as $(\bar{1}\,2\,\bar{1}\,1)_3$, where the positive number means the number of right stacking layers,

Table 3. Expressions and crystallographic parameters of polytypes of LPSO structures in Mg–M–RE alloys.

Type	Ramsdell symbols	Stacking sequences Jagodzinski notations	Zhdanov symbols	New symbols	*c* (nm)	Space groups	Ref.
F-type	10H	AB′C′ACAC′B′AB *hcchhhcchh*	$(\bar{1}\,3\,\bar{1}\,1\,\bar{3}\,1)$	$(F1\bar{1}1)$	2.61	$P6_3/mmc$	Luo et al. [13]
	18R	AB′C′ACACA′B′CBCBC′A′BAB *hcchhhhcchhhhcchhh*	$(\bar{1}\,3\,\bar{1}\,1)_3$	$(F2)_3$	4.69	$R\bar{3}m$	
	14H	AB′C′ACACAC′B′ABAB *hcchhhhhcchhhh*	$(\bar{1}\,3\,\bar{1}\,1\,\bar{1}\,1\,\bar{3}\,1\,\bar{1}\,1)$	$(F3\bar{F}3)$	3.65	$P6_3/mmc$	Matsuda et al. [9]
	24R	AB′C′ACACACA′B′CBCBCBC′A′BABAB *hcchhhhhhcchhhhhhcchhhhh*	$(\bar{1}\,3\,\bar{1}\,1\,\bar{1}\,1)_3$	$(F4)_3$	6.25	$R\bar{3}m$	
T-type	15R	AB′CBC BC′ACA CA′BAB *hchhhhchhhhchhh*	$(\bar{1}\,2\,\bar{1}\,1)_3$	$(T2)_3$	3.91	$R\bar{3}m$	Mi and Jin [14]
	12H	AB′CBCBCB′ABAB *hchhhhhchhhh*	$(\bar{1}\,2\,\bar{1}\,1\,\bar{1}\,1\,\bar{2}\,1\,\bar{1}\,1)$	$(T3\bar{T}3)$	3.13	$P6_3/mmc$	
	21R	AB′CBCBCBC′ACACACA′BABAB *hchhhhhhchhhhhhchhhhh*	$(\bar{1}\,2\,\bar{1}\,1\,\bar{1}\,1)_3$	$(T4)_3$	5.47	$R\bar{3}m$	
FT-type	51R	AB′CBCBC′A′BABAB′C′ACA **C…**		$[(T2F2F)2]_3$	13.3	$R\bar{3}m$	Present work
	72R	AB′CBCBC′A′BABAB′C′ACACAC′BCBC **B…**		$[(T2F2F)3(\bar{T})3]_3$	18.8	$R3m$	
	29H	AB′CBCBC′A′BABAB′C′ACACAC′BCBCB′ABAB **A…**		$(T2F2F)3(\bar{T}2\bar{T})3$	7.55	$P3m1$	
	102R	AB′CBCBC′A′BABAB′C′ACACAC′BCBCB′ABA BA′C ACA **C…**		$[(T2F2F)3(\bar{T}2\bar{T}2\bar{T})3]_3$	26.6	$R3\ m$	
	192R	AB′CBCBC′A′BABAB′C′ACACAC′BCBCB′ABAB AB′CBCBC′A′BABAB′C′ACACAC′BCBC BC′ACACA′B′CBC **B…**		$[(T2F2F)3(\bar{T}2\bar{T})3\ (T2F2F)3(\bar{T})3(T2F2)]_3$	50.0	$R3\ m$	
	60H	AB′C′AC AC′B′ABAB $(AB′CBCB\ CB′ABAB)_4$ **A…**		$(F1\bar{F}1)2(T3\bar{T}3)_4$	15.6	$P\bar{6}m2$	

the negative number means the number of fault stacking layers, and the subscript number 3 indicates three repeated sub unit cells with the same size and symmetry in one 15R unit cell.

Actually the above-mentioned notations are not convenient to describe the LPSO structures with ultra-long period. Here, we introduce a new notation to characterise the stacking sequence of the LPSO structures in the present Mg-alloy, which contains both AB′C′A and AB′C building blocks. The rules are as follow: AB′C′A (and/or AC′B′A) building block consisting of four layers are defined as F-block and denoted as F (and/or $\bar{\text{F}}$); while AB′C (and/or AC′B) building block consisting of three layers are defined as T-block and denoted as T (and/or $\bar{\text{T}}$), where the bar sign presents the opposite shear direction of the block. The n (n = integer) means the number of Mg layers sandwiched between the F and/or T, written as n-Mg; The subscript number is employed to present the number of sub unit cells with same size and symmetry. For example, the 15R structure can be expressed as $(\text{T2})_3$ and 12H as (T3 $\bar{\text{T}}$3) by the new notations. All the LPSO structures in the Mg alloys are classified into three types. They are F-type, T-type and FT-type (F and T mixed type), respectively, as labelled in Table 3.

In order to identify the M/RE elements distribution in the different layers of an LPSO structure, it is necessary to distinguish one basal layer from another in a (sub) unit cell. For convenience, we use the Jagodzinski notations for intensity analysis. The c stacking layers in T- and F-block are denoted as c^{T} and c^{F}, while the h layers that are in the first, second and third nearest neighbour to c^{T} (c^{F}) layers are denoted as h_1^{T}, h_2^{T} and h_3^{T} (h_1^{F}, h_2^{F} and h_3^{F}), respectively. We define relative intensity of a layer in the Z-contrast profile of HAADF-STEM images as the ratio of average peak value of one layer (I) to that of h_2 layer, designated as I/I_{h_2}. Thus, the relative intensity of c^{T}, h_1^{T}, h_2^{T} and h_3 (c^{F}, h_1^{F} and h_2^{F}) layers are $\text{I}_{c^{\text{T}}}/\text{I}_{h_2}$, $\text{I}_{h_1^{\text{T}}}/\text{I}_{h_2}$, $\text{I}_{h_2^{\text{T}}}/\text{I}_{h_2}$ and $\text{I}_{h_3}/\text{I}_{h_2}$, ($\text{I}_{c^{\text{F}}}/\text{I}_{h_2}$, $\text{I}_{h_1^{\text{F}}}/\text{I}_{h_2}$ and $\text{I}_{h_2^{\text{F}}}/\text{I}_{h_2}$), respectively.

3. Experiments

The graphite crucible was used under protection of ultrahigh purity argon atmosphere in a high frequency induction melting furnace. The ingots of a Mg–Co–Y alloy with the nominal composition of Mg-2.0at.% Co-6.0at.% Y were prepared by melting the high purity Mg, Mg-30 wt.% Y and Co_5Y_8 master ingots and cooled down to the room temperature in the furnace. The microstructure of the as-cast alloys was first investigated by scanning electron microscopy (SEM), and the local chemical compositions were measured using energy-dispersive X-ray spectroscopy (EDX) in SEM. Thin foils for TEM and STEM observations were prepared by grinding, polishing, dimpling and Ar ion milling in a Gatan precision ion polishing system. The thinning rate was gradually reduced during the final stage to produce a wide thin area for high resolution microscopic observation. A Tecnai G^2 F30 transmission electron microscope is used for getting bright-field (BF) images and SAED patterns. An aberration-corrected Titan$^{3\text{TM}}$ G^2 60-300 scanning transmission electron microscopes equipped with a high-brightness field-emission gun (X-FEG) and double Cs correctors from CEOS was used for atomic-scale imaging and composition analysis. The convergence angle of the electron beam is 25 mrad in the STEM mode, which yields a probe size of less than 0.10 nm.

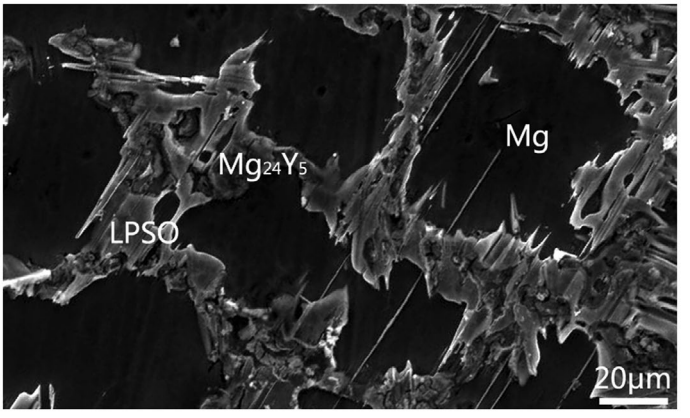

Figure 2. A BSE – SEM micrograph showing the typical microstructure of the $Mg_{92}Co_2Y_6$ (at.%) as-cast alloy.

4. Results

4.1. The microstructure of $Mg_{92}Co_2Y_6$ (at.%) as-cast alloy

A BSE SEM image of the typical microstructure of $Mg_{92}Co_2Y_6$ (at.%) as-cast alloy is presented in Figure 2, in which the contrast of each phase depends on its chemical composition. The grain size ranges from 50 to 150 μm, and intermetallic particles are visible along the grain boundaries. The dominant second phases, LPSO structure and $Mg_{24}Y_5$ intermetallic phase, show white contrast in the as-cast alloy. The contents of $MgYCo_4$ and $Mg_3(Co, Y)$ intermetallic phases [28,29] are much less than those in the $Mg_{88}Co_5Y_7$ as-cast alloy [14]. In addition, EDX measurement revealed that the average chemical composition of the LPSO structures in this alloy is $Mg_{87-88}Co_{2-3}Y_{9-10}$ (at.%), which is different from that $Mg_{89-92}Co_{2-4}Y_{6-7}$ (at.%) in $Mg_{88}Co_5Y_7$ as-cast alloy [14]. The difference should be strongly related to the distinguished Co/Y ratio in these two alloys. In this work, we focused on investigating the crystallographic features of new LPSO structures containing both F-blocks and T-blocks using atomic-resolution HAADF-STEM.

4.2. The 72R and 102R LPSO structures

Figure 3(a) is a low-magnification bright-field TEM image showing co-existence of several LPSO structures and Mg matrix. Figure 3(b) shows the SAED pattern of the LPSO structure in Region I (R I), taken with the incident beam parallel to the $[2\ \bar{1}\ \bar{1}\ 0]_\alpha$ zone axis, where the subscript α represents the Mg matrix. The extra diffraction spots in the SAED pattern appear at positions $n/24(0\ 0\ 0\ 2)_{Mg}$ (n is an integer), indicating that it is either 24H or 72R structure, based on the analysis of the diffraction patterns of closely packed ordered structures listed in Table 2. As the $(0\ \bar{1}\ 1\ 0)$ spot does not appear, the LPSO structure was determined as rhombohedral Bravias lattice with 72 layers and named as 72R. The $(0\ \bar{1}\ 1\ l)$, $(0\ 0\ 0\ l)$ and $(0\ 1\ \bar{1}\ l)$ spots are indexed as $(0\ \bar{1}\ 1\ 3n+1)_{72R}$ (n is an integer), $(0\ 0\ 0\ 3n)_{72R}$, and $(0\ 1\ \bar{1}\ 3n\text{-}1)_{72R}$ in hexagonal coordinate, respectively. The lattice parameters of 72R structure are $a = 0.321$ nm and $c = 18.8$ nm, which are derived by $a_{72R} = a_{Mg}$ and $c_{72R} = \frac{1}{2}72c_{Mg}$ in accordance with the data measured by SAED patterns. Figure 3(d) is an SAED pattern of the LPSO structure in Region II (R II), taken along the $[2\ \bar{1}\ \bar{1}\ 0]_\alpha$ direction. The extra

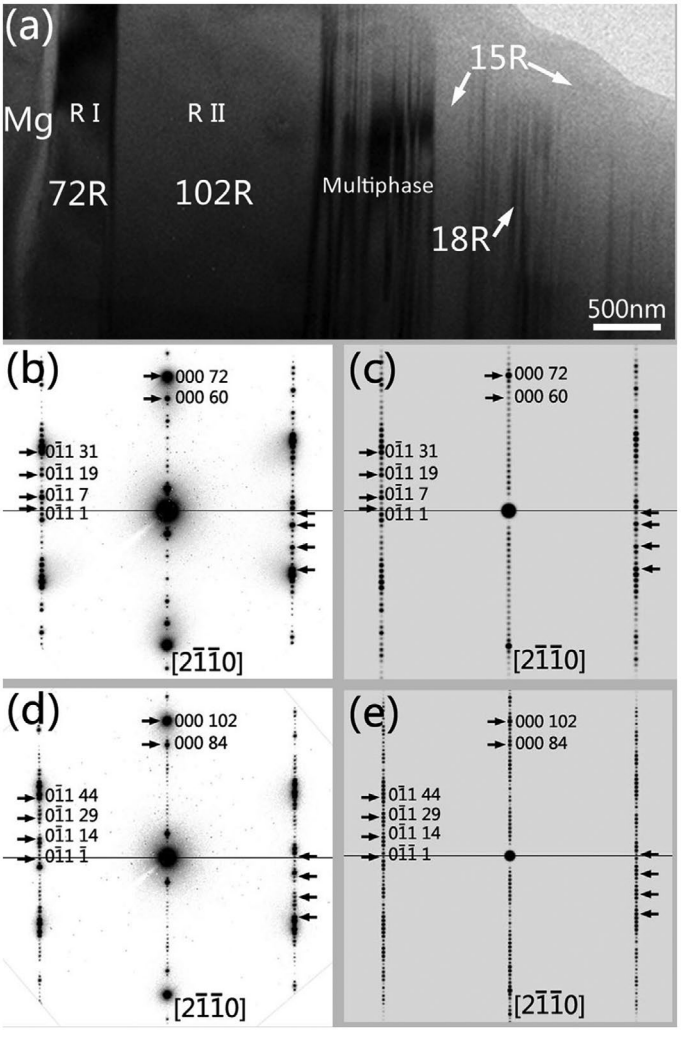

Figure 3. (a) A low magnification TEM image showing Mg, 72R, 102R, 15R, 18R, and multiply phases coexisting with each other in the $Mg_{92}Co_2Y_6$ as-cast alloy. (b) Experimental and (c) simulated SAED patterns of the 72R structure, obtained along the $[2\,\bar{1}\,\bar{1}\,0]_\alpha$ zone axis. (d) Experimental and (e) simulated SAED patterns of the 102R structure, obtained along the $[2\,\bar{1}\,\bar{1}\,0]_\alpha$ zone axis.

diffraction spots are located at the positions of $n/34(0002)_{Mg}$ (n is an integer), and the $(0\,\bar{1}\,1\,0)$ spot is invisible. Thus, this LPSO structure can be determined as 102R. Similarly, the $(0\,\bar{1}\,1\,l)$, $(0\,0\,0\,l)$ and $(0\,1\,\bar{1}\,l)$ spots can be indexed as $(0\bar{1}1\ 3n+1)_{102R}$, $(000\ 3n)_{102R}$ and $(01\bar{1}\ 3n-1)_{102R}$ (n is an integer), respectively. The lattice parameters of the 102R structure are derived as $a_{102R} = a_{Mg} = 0.321$ nm and $c_{102R} = \frac{1}{2}102c_{Mg} = 26.6$ nm.

The SAED patterns of 72 and 102R structures along the $[2\,\bar{1}\,\bar{1}\,0]_\alpha$ zone axis were simulated with stacking sequence of the 72 and 102R structures, shown in Figure 3(c) and (e), respectively. The distribution of diffraction spots in the simulated SAED patterns agree well with that in the experimental patterns (Figure 3(b) and (d)).

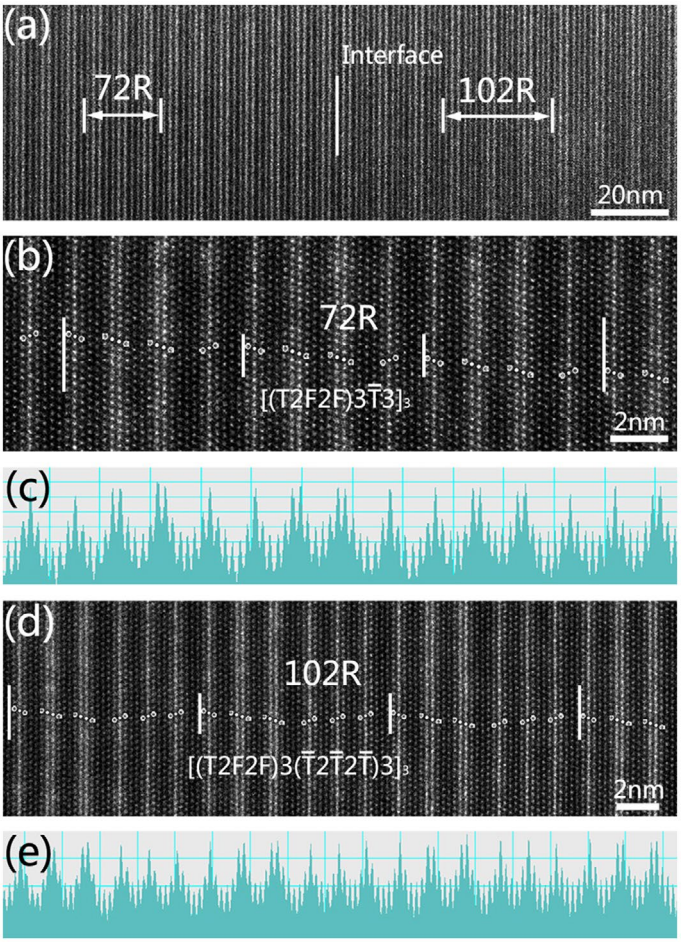

Figure 4. (colour online) (a) A low magnification HAADF-STEM image of the coexisting 72R and 102R structures. Atomic resolution HAADF-STEM images of (b) 72R and (d) 102R structures. (c) and (e) Intensity profiles of the HAADF-STEM image in (b) and (d), respectively. These images are obtained with the electron beam parallel to $[2\,\bar{1}\,\bar{1}\,0]_{\alpha}$ zone axis.

Figure 4(a) shows a low magnification STEM image of 72R and 102R structures obtained with the electron beam parallel to $[2\,\bar{1}\,\bar{1}\,0]_{\alpha}$ zone axis. It is confirmed that the brighter ones are F-blocks while the weaker ones are T-blocks, as seen in Figure 4(b)–(d). Two F-block and two T-block are stacked alternately in the 72R along the stacking direction. In contrast, two F-block and four T-block are present alternately in the 102R. Figure 4(b) is a typical atomic-resolution HAADF-STEM image of the 72R structure, viewed along the $[2\,\bar{1}\,\bar{1}\,0]_{\alpha}$ zone axis. The sub unit cells of 24 layers share the same size and symmetry but are shared with respect to each other by a Shockley Burgers vector. The stacking sequence of the first sub unit cell is AB′CBCBC′A′BABAB′C′ACACAC′BCBC (**B…**). If we assume the atoms in the 1st layer are at positions of A, the atoms in the 25th, 49th, and 73th layers are at positions of B, C and again A, respectively. Thus, the 72R LPSO structure can be expressed as $[(\mathrm{T2F2F})3(\bar{\mathrm{T}})3]_3$. Figure 4(c) is the Z-contrast intensity profile of each stacking layer obtained from the image in Figure 4(b). According to the above definition, the sub structure unit of

72R, AB′CBCBC′A′BABAB′C′ACACAC′BCBC, can also be expressed by the Jagodzinski notations as $h_1^{\mathrm{T}}\mathbf{c}^{\mathbf{T}}h_1^{\mathrm{T}}h_2^{\mathrm{T}}h_2^{\mathrm{F}}h_1^{\mathrm{F}}\mathbf{c}^{\mathbf{F}}\mathbf{c}^{\mathbf{F}}h_1^{\mathrm{F}}h_2^{\mathrm{F}}h_2^{\mathrm{F}}h_1^{\mathrm{F}}\mathbf{c}^{\mathbf{F}}\mathbf{c}^{\mathbf{F}}h_1^{\mathrm{F}}h_2^{\mathrm{F}}h_3h_2^{\mathrm{T}}h_1^{\mathrm{T}}\mathbf{c}^{\mathbf{T}}h_1^{\mathrm{T}}h_2^{\mathrm{T}}h_3h_2^{\mathrm{T}}$. Obviously, I_{c^T} and I_{c^F} are approximately of the same value, and the Z-contrast intensity distribution of the left and right of the c^T or c^F layers is roughly symmetric. That is $I_{c^T} > I_{h_1^T} > I_{h_2^T} > I_{h_3^T}$ and $I_{c^F} > I_{h_1^F} > I_{h_2^F} > I_{h_3^F}$, which suggests that the content of Co/Y elements decreases in the range of c, h_1, h_2 and h_3 layers.

Figure 4(d) displays a typical atomic-resolution HAADF-STEM image of the 102R structure, viewed along the $[2\,\bar{1}\,\bar{1}\,0]_\alpha$ zone axis. Similar to 72R, the sub unit cells of 34 layers share the same size and symmetry but are sheared with respect to each other by a Shockley Burgers vector in the 102R. The stacking sequence of the first sub unit cell is: AB′CBCBC′A′BABAB′C′ACACAC′BCBCB′ABABA′CACA (**C…**). The atoms in the 1st, 35th, 69th layer are at positions of A, C and B, respectively, while those in the 103th layer are at positions of A which is the same as those in the first layer. Hence, the 102R LPSO structure can be expressed as $[(\mathrm{T2F2F})3(\bar{\mathrm{T}}2\bar{\mathrm{T}}2\bar{\mathrm{T}})3]_3$. Figure 4(e) displays the intensity profile of the image in Figure 4(d), which suggests the elements distribution in each layer of 102R is similar to that of 72R in Figure 4(c). As demonstrated in Figures 4(b) and 3(d), no symmetric operations exist, nor any clusters is regularly aligned in the basal planes of 72 and 102R LPSO structures, so the space group of 72 and 102R structures could be determined as *R*3*m*.

4.3. The 29H and 192R LPSO structure

Figure 5(a) is a low magnification HAADF-STEM image obtained along the $[2\,\bar{1}\,\bar{1}\,0]_\alpha$ zone axis, which displays the intergrowth of 15R, 18R and two other LPSO structures. The SAED pattern of Region I is shown in Figure 5(b), taken with the incident beam parallel to the $[2\,\bar{1}\,\bar{1}\,0]_\alpha$ zone axis. The extra diffraction spots in the SAED pattern are visible at positions $n/29(0002)_{\mathrm{Mg}}$ (n is an integer) and the $(0\,\bar{1}\,1\,0)$ spot is also visible. Thus, the LPSO structure in Region I can be labelled as 29H. The $(0\,\bar{1}\,1\,l)$, $(0\,0\,0\,l)$ and $(0\,1\,\bar{1}\,l)$ array can be indexed as $(0\,\bar{1}\,1\,n)_{29\mathrm{H}}$ (n is an integer), $(0\,0\,0\,n)_{29\mathrm{H}}$, and $(0\,1\,\bar{1}\,n)_{29\mathrm{H}}$ in hexagonal coordinate. The lattice parameters of the 29H structure are derived as $a_{29\mathrm{H}} = a_{\mathrm{Mg}} = 0.321$ nm and $c_{29\mathrm{H}} = \frac{1}{2}29c_{\mathrm{Mg}} = 7.55$ nm. A typical atomic-resolution HAADF-STEM image of the 29H structure is shown in Figure 5(d), viewed along the $[2\,\bar{1}\,\bar{1}\,0]_\alpha$ zone axis. There exist unit cells of 29 layers with stacking sequence of AB′CBCBC′A′BABAB′C′ACACAC′BCBCB′ABAB (**A…**). The atoms in the 1st and 30th layer are both at position A. The 29H LPSO structure here can be expressed as $(\mathrm{T2F2F})3(\bar{\mathrm{T}}2\bar{\mathrm{T}})3$. Based on the structural model of pure Mg with stacking sequence of the 29H structure, the simulated diffraction pattern (Figure 5(c)) matches well with that obtained in the experiment (Figure 5(b)).

Figure 5(e) is an atomic-resolution HAADF-STEM image of another new LPSO structure with ultra-long period in Region II of Figure 5(a). The sub unit cell of 64 layers with stacking sequence of AB′CBCBC′A′BABAB′C′ACACAC′BCBCB′ABAB AB′CBCBC′A′BABAB′C′ACACAC′BCBC BC′ACACA′B′CBC (**B…**) is identified. The positions of atoms in the 1st, 65th, 129th and 193th layers are A, B, C and A, respectively. Thus, this structure is the 192R LPSO and can be expressed simply as $[(\mathrm{T2F2F})3(\bar{\mathrm{T}}2\bar{\mathrm{T}})3(\mathrm{T2F2F})3(\bar{\mathrm{T}})3(\mathrm{T2F2})]_3$ by the symbols introduced in this study. It is seen that the substructure of 192R includes substructure of 29H and 72R LPSO structures, e.g. $(\mathrm{T2F2F})3(\bar{\mathrm{T}}2\bar{\mathrm{T}})3$ and $(\mathrm{T2F2F})3(\bar{\mathrm{T}})3$, respectively. The 192R LPSO structure consists of three sub unit cells with 64 layers, and the lattice parameters of 192R structure are $a_{192\mathrm{R}} = a_{\mathrm{Mg}} = 0.321$ nm

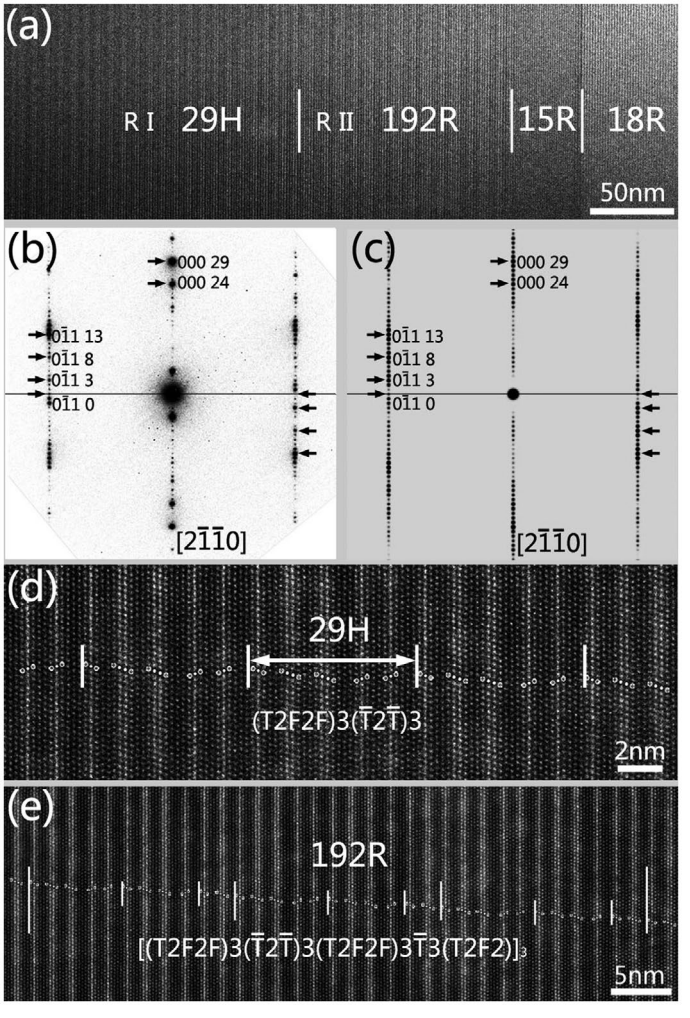

Figure 5. (a) A low magnification HAADF-STEM image of the intergrowth of 29H, 192R, 15R and 18R structures (b) Experimental and (c) simulated SAED pattern of the 29H structure. Atomic resolution HAADF-STEM images of (d) 29H structure and (e) 192R structure. All of those images were obtained along the $[2\bar{1}\bar{1}0]_\alpha$ zone axis.

and $c_{192R} = \frac{1}{2}192c_{Mg} = 50$ nm. Analogous to the 72R and 102R structures, symmetric operation and ordered clusters do not exist along basal plane in 29H and 192R structures, their space group can be derived as $P3m1$ and $R3m$, respectively.

4.4. The 51R and 60H LPSO structure

In addition to the above-mentioned 72R, 29H, 102R and 192R structures coexisting with 15 and 18R structures, another two LPSO structures adjacent to grain boundaries are also identified. Figure 6(a) displays a low-magnification HAADF image of the LPSO structures in two grains with the electron beam parallel to $[2\bar{1}\bar{1}0]_\alpha$ zone axis. The bright fringe lines with relative wider thickness are F-block and the bright ones with narrower thickness are T-block.

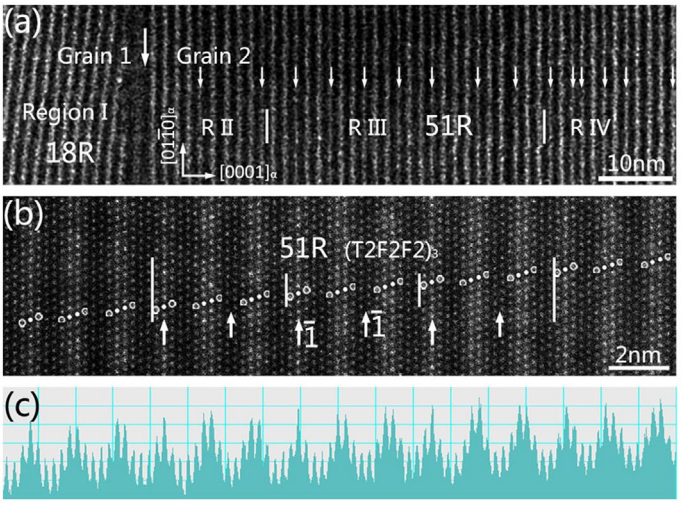

Figure 6. (colour online) (a) An HAADF-STEM image showing the microstructure containing both F-blocks and T-blocks at the grain boundary of 18R structure in the as-cast $Mg_{92}Co_2Y_6$ alloy. (b) An atomic-resolution HAADF-STEM image of the 51R structure. (c) Z-contrast intensity profiles of the HAADF image in (b). These images are obtained with the electron beam parallel to $[2\bar{1}\bar{1}0]_\alpha$ zone axis.

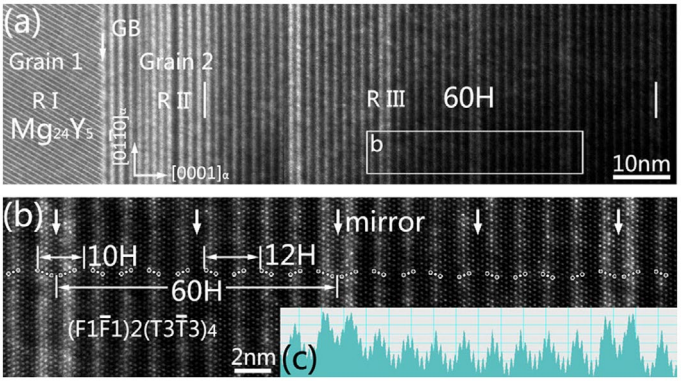

Figure 7. (colour online) (a) A low magnification HAADF-STEM image of another microstructure containing both F-blocks and T-blocks at the grain boundary of $Mg_{24}Y_5$ in the as-cast $Mg_{92}Co_2Y_6$ alloy. (b) An atomic-resolution HAADF-STEM image of the region framed in (a), implying the stacking sequence of 60H. (c) Z-contrast intensity profiles across different parts of the 60H. These images were obtained with the electron beam parallel to $[2\bar{1}\bar{1}0]_\alpha$ zone axis of the structure in Grain 2.

The image can be divided into three regions according to the distribution of building blocks: Region I is 18R structure, Region II is disordered structure, while Region III features an alternate array of two F-block and one T-block. The atomic resolution HAADF-STEM image of R III is shown in Figure 6(b). A sub unit cell of 17 layers with stacking sequence of AB′CBCBC′A′BABAB′C′ACACAC′BCBC (**B…**) is identified. The positions of atoms in the 1st, 18th, 35th and 52th layers are A, C, B and A, respectively. Therefore, the structure is 51R and can be expressed as $[(T2F2F)2]_3$ by the symbols introduced in this study. The lattice parameters of 51R structure are $a_{51R} = a_{Mg} = 0.321$ nm and $c_{51R} = \frac{1}{2}51c_{Mg} = 13.3$ nm.

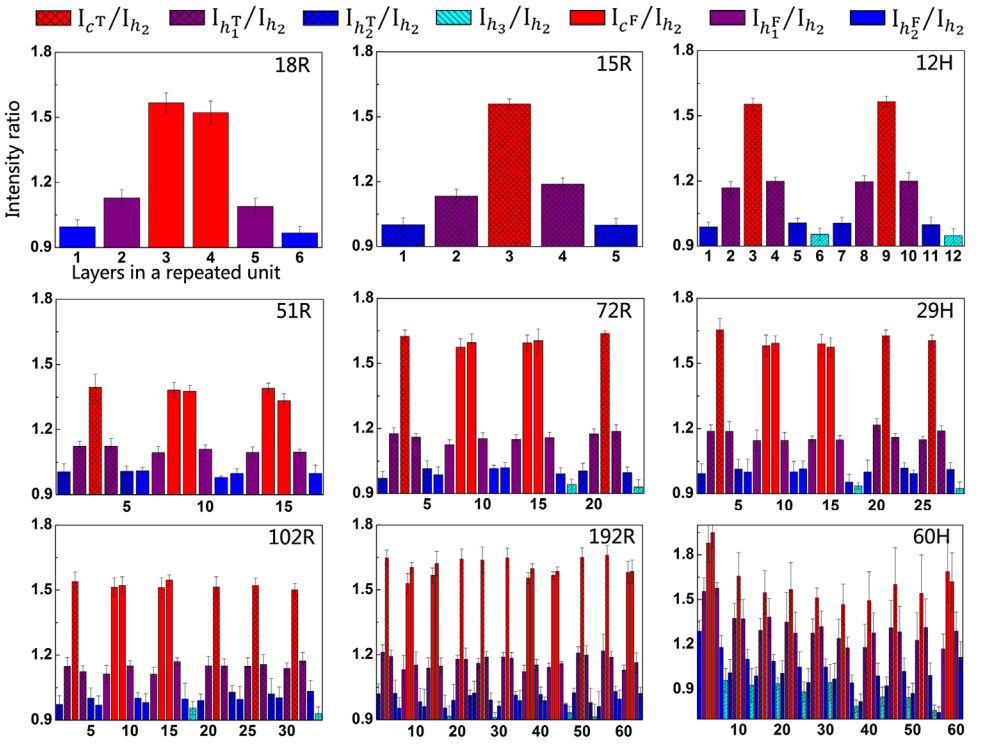

Figure 8. (colour online) The relative intensity ratio histogram of c^T, h_1^T, h_2^T and h_3 (c^F, h_1^F and h_2^F) layers in HAADF-STEM images for the subunit of 18R, 15R, 12H, 51R, 72R, 29H, 102R, 192R and 60H, which is noted as I_{c^T}/I_{h_2}, $I_{h_1^T}/I_{h_2}$, $I_{h_2^T}/I_{h_2}$ and I_{h_3}/I_{h_2}, (I_{c^F}/I_{h_2}, $I_{h_1^F}/I_{h_2}$ and $I_{h_2^F}/I_{h_2}$).

It is worthwhile to mention that there is an inversion centres $\bar{1}$ in the basal layers marked with arrows in Figure 6(b). Based on the crystallography, the space group of the 51R structure can be derived as $R\bar{3}m$. Figure 6(c) shows Z-contrast intensity profile of Figure 6(b). The characteristic of element distribution in each layer of the 51R is similar to that of 72R in Figure 4(b)–(c).

A low-magnification HAADF-STEM image of another grain boundary in the as-cast $Mg_{92}Co_2Y_6$ alloy is shown in Figure 7(a), where the bright fringe lines with wider thickness are F-block and the ones with narrower thickness are T-block. The image can be divided into three regions according to the distribution of the blocks. Region I is $Mg_{24}Y_5$ structure, while Region II features a random arrangement of the F-block and T-block. However, Region III is composed of an alternate array of F-block pairs and eight T-blocks. The stacking sequence of the structure in Region III is determined as AB′C′ACAC′B′ABAB(AB′CBCB CB′ABAB)$_4$ (**A…**), as seen in Figure 7(b). This structure corresponds to 60H and can be expressed as (F1$\bar{1}$F 1)2(T3$\bar{1}$T3)$_4$, which is also considered as the ordered arrangement of one 10H cell and four 12H cells [9,10,14] The lattice parameters of the 60H structure are $a_{60H} = a_{Mg} = 0.321$ nm and $c_{60H} = \frac{1}{2}60c_{Mg} = 15.6$ nm. Since the mirror plane $m_\perp$ and the reversion centre of $\bar{6}$ are present (marked with the arrows in Figure 7(b)), the space group of the 60H structure can be derived as $P\bar{6}m2$. Figure 7(c) shows the Z-contrast intensity profile of each layer of the 60H structure in Figure 7(b). It is seen that that $I_{c^F} > I_{c^T}$ and $I_{h_1^F} > I_{h_1^T}$ which indicates that

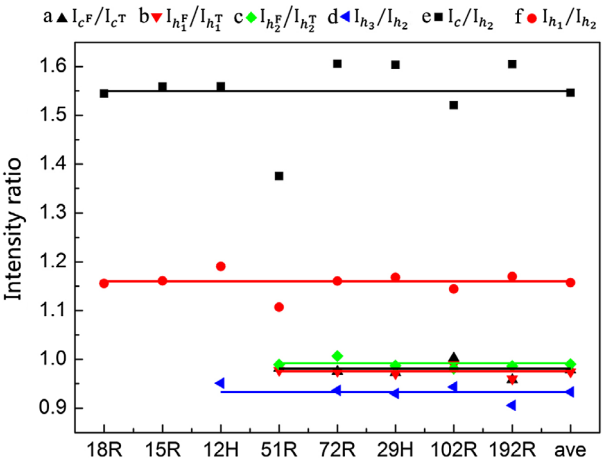

Figure 9. (colour online) (a–c) Intensity ratio I_{c^F}/I_{c^T}, $I_{h_1^F}/I_{h_1^T}$ and $I_{h_2^F}/I_{h_2^T}$ of 51R, 72R, 29H, 102R and 192R LPSO structures. (d-f) The relative intensity of *c* layers, h_1 layers and h_3 layers in various LPSO structures.

the content of Co/Y elements in c^F and h_1^F layers of the 60H is higher than that in c^T and h_1^T layers, respectively. This is a little bit different from the element distribution in that shown in Figure 4(c) and (e).

5. Discussion

5.1. The chemical feature of Co/Y elements along the c-axis of LPSO structures

To study the distribution of the M/RE elements in the basal layers of various LPSO structures in $Mg_{92}Co_2Y_6$ alloys, we focus on the relative intensity of the basal layers based on the atomic-resolution HAADF-STEM images, as shown by the intensity ratio histogram in Figure 8. The *c* stacking layers in T- and F-block are denoted as c^T and c^F, while the *h* layers that in the first, second and third nearest neighbour to c^T (c^F) layers are denoted as h_1^T, h_2^T and h_3^T (h_1^F, h_2^F and h_3^F), respectively. The distribution of Co/Y elements shows symmetrical on the left and right side of c^T and c^F layers. It is also seen that $I_{c^T}/I_{h_2} > I_{h_1^T}/I_{h_2} > I_{h_2^T}/I_{h_2} > I_{h_3^T}/I_{h_2}$ and $I_{c^F}/I_{h_2} > I_{h_1^F}/I_{h_2} > I_{h_2^F}/I_{h_2} > I_{h_3^F}/I_{h_2}$, which suggests the content of Co/Y decreases in the *c*, h_1 and h_2 layers. The distribution of the M/RE elements in the range of c^F, h_1^F and h_2^F layers is in accordance with the counterpart in 18R structure in $Mg_{97}Zn_1Y_2$ (at.%) alloys [17], in which the Zn_6Y_8 cluster is believed to be arranged in short-range order in the basal planes. Based on the highly ordered structure models [11,12,18], the number of atoms in $2\sqrt{3}a_{Mg} \times 2\sqrt{3}a_{Mg}$ unit cell are described as *c* layer (6Mg, 3M, 3RE), h_1 layer (11Mg, 1RE) and h_2 layer (12Mg). Then the distribution of the M/RE elements in different layers would result in $I_{c^F}/I_{h_2} > I_{h_1^F}/I_{h_2} > I_{h_2^F}/I_{h_2}$. It is worthwhile to mention that $I_{h_2^F}/I_{h_2}$ should be equal to $I_{h_3^F}/I_{h_2}$, since the h_2 and h_3 layers are only occupied with Mg [15]. However, in the LPSO structures of the present Mg–Co–Y alloys, $I_{h_2} > I_{h_3}$. This implies that more M/RE atoms are present in h_2 than in h_3 layer.

The profiles in Figure 9(a)–(c) show the value of I_{c^F}/I_{c^T}, $I_{h_1^F}/I_{h_1^T}$ and $I_{h_2^F}/I_{h_2^T}$ extracted from five FT-type LPSO structures, namely, 51R, 72R, 29H, 102R and 192R structures. The values range from 0.97 to 1.00. It is seen that the mean intensity of c^T, h_1^T and h_2^T layer are

approximately equal to the counterpart of c^{F}, h_1^{F} and h_2^{F} layer. In the following discussion, $I_{c^{F}}$ and $I_{c^{T}}$, $I_{h_1^{F}}$ and $I_{h_1^{T}}$, $I_{h_2^{F}}$ and $I_{h_2^{T}}$ will not be distinguished. They are simplified as I_c, I_{h_1} and I_{h_2}, respectively. The relative intensity of c, h_1 and h_3 layers in various LPSO structures are displayed in Figure 9(d)–(f). The fluctuation of the chemical compositions is mainly due to the intrinsic disorder of Co/Y atoms in the basal plane. The slight discrepancy in the relative intensities of 51R and 60H is proposed to result from the segregation of solute atoms close to the grain boundary (Figure 8).

5.2. The distribution of Co/Y elements in the basal planes of LPSO structures

In the Mg–M–RE (M = Al, Ni, Cu and Zn; RE = Y and Gd) ternary systems [6–13], the heat of mixing [24] between two elements is: $\Delta H^{\mathrm{mix}}_{\mathrm{Mg-RE}} = -6\mathrm{kJ/mol}$, $-4\mathrm{kJ/mol} < \Delta H^{\mathrm{mix}}_{\mathrm{Mg-M}} < -2\mathrm{kJ/mol}$, $-38\mathrm{kJ/mol} < \Delta H^{\mathrm{mix}}_{\mathrm{M-RE}} < -22\mathrm{kJ/mol}$. Thus, the M and RE elements are more likely to bond together. Moreover, the diameter of Mg, M and RE atoms lines up $r_{\mathrm{M}}(0.124{-}0.143)\mathrm{nm} < r_{\mathrm{Mg}}(0.16)\,\mathrm{nm} < r_{\mathrm{RE}}(0.18)\,\mathrm{nm}$, so the combination of M and RE atoms can minimise the compression strain associated with RE atoms and the extension strain associated with M atoms. It has been experimentally observed that Zn_6RE_8 or Zn_6RE_8 (Mg, Zn, RE) clusters are regularly aligned in the $2\sqrt{3}a_{\mathrm{Mg}} \times 2\sqrt{3}a_{\mathrm{Mg}}$ unit cell [18,25] within the in-plane ordered LPSO structures in Mg–Zn–RE alloys. They were further rationalised based on the first principle calculations [26,27]. These clusters give rise to superlattice spots or streaks in $1/2(0\ 1\ \bar{1}\ l)$ and $n/6(1\ 1\ \bar{2}\ l)$ reciprocal lattice rows in the SAED patterns along the $[2\ \bar{1}\ \bar{1}\ 0]_{\alpha}$ and $[1\ 0\ \bar{1}\ 0]_{\alpha}$ directions. Concerning the atoms diameter and mixing heat of Co and Y, we propose that Co and Y elements may form clusters due to $r_{\mathrm{Co}}(0.126)\,\mathrm{nm} < r_{\mathrm{Mg}} < r_{Y}$ and $\Delta H^{\mathrm{mix}}_{\mathrm{Co-Y}} = -22\mathrm{kJ/mol}$ in Mg–Co–Y alloy. The Co and Y atoms are actually segregated in the basal planes, e.g. B′ and B′C′ planes in the AB′C and AB′C′A blocks, respectively, as shown in atomic resolution STEM images in Figures 3–6. Nonetheless, as shown in Figures 3(b), (d) and 5(b), neither superlattice spots nor streaks were observed between $(0\ 0\ 0\ l)$ and $(0\ 1\ \bar{1}\ l)$ rows in the SAED patterns along $[2\ \bar{1}\ \bar{1}\ 0]_{\alpha}$ zone axis of various LPSO phases. This may imply that the Co and Y clusters distribute in disordered fashion in the basal planes of this Mg–Co–Y alloy.

Evident ordered clusters are not detected in the basal planes of FT-type LPSO structures in the present study, which indicates that the primitive 3-fold symmetry is not destroyed. Further, there is no extra symmetric operation in 72R, 29H, 102R and 192R structures, so their space groups are derived as $R3m$, $P3m1$, $R3m$ and $R3m$, respectively. In contrast, symmetric operation $\bar{1}$ and $m_{\perp}$ remain in 51R and 60H, making their space groups as $R\bar{3}m$ and $P\bar{6}m2$, respectively.

6. In summary

Based on Cs-corrected HAADF-STEM imaging at the atomic level, we have determined the structures and elemental distribution of six new polytypes of LPSO structures in as-cast $Mg_{92}Co_2Y_6$ (at.%) alloys. We summarise as follows:

(1) Each of the observed new LPSO structures, 29H, 51R, 60H, 72R, 102R, and 192R, is composed of both AB′C′A (F-block) and AB′C (T-block) building blocks.

(2) The unit cells and space groups of the six new LPSO structures are formulated as: 72R, $[(T2F2F)3(\bar{T})3]_3$, *R3m*; 29H, $(T2F2F)3(\bar{T}2\bar{T})3$, *P3m*1; 102R, $[(T2F2F)3(\bar{T}2\bar{T}2\bar{T})3]_3$, *R3m*; 192R, $[(T2F2F)3(\bar{T}2\bar{T})3(T2F2F)3(\bar{T})3(T2F2)]_3$, *R3m*; 51R, $[(T2F2F)2]_3$, $R\bar{3}m$; 60H, $(F1\bar{F}1)2(T3\bar{T}3)_4$, $P\bar{6}m2$. The lattice parameter of each LPSO structure is derived as: $a_{LPSO} = a_{Mg} = 0.321$ nm and $c_{LPSO} = \frac{1}{2}n \times c_{Mg}$ (n = integer, corresponding to 72, 29, 102, 192, 51 and 60).

(3) The Co/Y elements are present in a disordered fashion in the basal planes of LPSO structures in the present Mg–Co–Y alloys. The distribution of Co/Y elements in the neighbouring layers of c^T and c^F layers are roughly symmetric in these LPSO structures, and the content of Co/Y elements decreases with the increase in the distance from the middle layer of AB′C′A and AB′C building blocks. In addition, for the 72R, 29H, 102R and 192R structures, $I_{c^F} = I_{c^T}$, $I_{h_1^F} = I_{h_1^T}$, $I_{h_2^F} = I_{h_2^T}$. In contrast, there are slight discrepancies in the intensity of 51R and 60H, which is proposed to result from the segregation of solute atoms in these structures near the grain boundary.

Acknowledgements

The authors are grateful to Prof S. J. Zheng and Dr Y. T. Zhou for fruitful discussion. We gratefully acknowledge Dr J. H. You and Prof K. Q. Qiu in Shenyang University of Technology for sample preparation.

Disclosure statement

No potential conflict of interest was reported by the authors.

Funding

This work is supported by the National Science Foundation of China [grant number 51301177]; The Innovation Fund of IMR [grant number SCJJ-2013-PY-08], [grant number 2015-PY08]; the Youth Fund of SYNL fund [grant number 2015FP18].

References

[1] A. Inoue, Y. Kawamura, M. Matsushita, K. Hayashi, and J. Koike, *Novel hexagonal structure and ultrahigh strength of magnesium solid solution in the Mg–Zn–Y system*, J. Mater. Res. 16 (2001), pp. 1894–1900.

[2] Y. Kawamura, K. Hayashi, A. Inoue, and T. Masumoto, *Rapidly solidifed powder metallurgy Mg97Zn1Y2 alloys with excellent tensile yield strength above 600 MPa*, Mater. Trans. 42 (2001), pp. 1171–1174.

[3] X.H. Shao, Z.Q. Yang, and X.L. Ma, *Strengthening and toughening mechanisms in Mg–Zn–Y alloy with a long period stacking ordered structure*, Acta Mater. 58 (2010), pp. 4760–4771.

[4] M. Yamasaki, N. Hayashi, S. Izumi, and Y. Kawamura, *Corrosion behavior of rapidly solidified Mg–Zn–rare earth element alloys in NaCl solution*, Corros. Sci. 49 (2007), pp. 255–262.

[5] J. Zhang, J. Xu, W. Cheng, C. Chen, and J. Kang, *Corrosion behavior of Mg–Zn–Y Alloy with long-period stacking ordered structures*, J. Mater. Sci. Technol. 28 (2012), pp. 1157–1162.

[6] Y. Kawamura, T. Kasahara, S. Izumi, and M. Yamasaki, *Elevated temperature Mg97Y2Cu1 alloy with long period ordered structure*, Scr. Mater. 55 (2006), pp. 453–456.

[7] Y. Kawamura and M. Yamasaki, *Formation and mechanical properties of Mg97Zn1RE2 alloys with long-period stacking ordered structure*, Mater. Trans. 48 (2007), pp. 2986–2992.
[8] T. Itoi, K. Takahashi, H. Moriyama, and M. Hirohashi, *A high-strength Mg–Ni–Y alloy sheet with a long-period ordered phase prepared by hot-rolling*, Scr. Mater. 59 (2008), pp. 1155–1158.
[9] M. Matsuda, S. Ii, Y. Kawamura, Y. Ikuhara, and M. Nishida, *Variation of long-period stacking order structures in rapidly solidified Mg97Zn1Y2 alloy*, Mater. Sci. Eng. A 393 (2005), pp. 269–274.
[10] E. Abe, A. Ono, T. Itoi, M. Yamasaki, and Y. Kawamura, *Polytypes of long-period stacking structures synchronized with chemical order in a dilute Mg–Zn–Y alloy*, Philos. Mag. Lett. 91 (2011), pp. 690–696.
[11] H. Yokobayashi, K. Kishida, H. Inui, M. Yamasaki, and Y. Kawamura, *Enrichment of Gd and Al atoms in the quadruple close packed planes and their in-plane long-range ordering in the long period stacking-ordered phase in the Mg–Al–Gd system*, Acta Mater. 59 (2011), pp. 7287–7299.
[12] K. Kishida, H. Yokobayashi, and H. Inui, *The most stable crystal structure and the formation processes of an order-disorder (OD) intermetallic phase in the Mg–Al–Gd ternary system*, Philos. Mag. 93 (2013), pp. 2826–2846.
[13] Z. Luo and S. Zhang, *High-resolution electron microscopy on the X-Mg12ZnY phase in a high strength Mg–Zn–Zr–Y magnesium alloy*, J. Mater. Sci. Lett. 19 (2000), pp. 813–815.
[14] S.-B. Mi and Q.-Q. Jin, *New polytypes of long-period stacking ordered structures in Mg–Co–Y alloys*, Scr. Mater. 68 (2013), pp. 635–638.
[15] K. Kishida, H. Yokobayashi, H. Inui, M. Yamasaki, and Y. Kawamura, *The crystal structure of the LPSO phase of the 14H-type in the Mg–Al–Gd alloy system*, Intermetallics 31 (2012), pp. 55–64.
[16] Q.-Q. Jin, C.-F. Fang, and S.-B. Mi, *Formation of long-period stacking ordered structures in Mg88M5Y7 (M=Ti, Ni and Pb) casting alloys*, J. Alloys Compd. 568 (2013), pp. 21–25.
[17] D. Egusa and E. Abe, *The structure of long period stacking/order Mg–Zn–RE phases with extended non-stoichiometry ranges*, Acta Mater. 60 (2012), pp. 166–178.
[18] M. Yamasaki, M. Matsushita, K. Hagihara, H. Izuno, E. Abe, and Y. Kawamura, *Highly ordered 10H-type long-period stacking order phase in a Mg–Zn–Y ternary alloy*, Scr. Mater. 78–79 (2014), pp. 13–16.
[19] K.X. Guo, H.Q. Ye, and Y.K. Wu, *Application of Electron Diffraction Patterns in Crystallography*, Science Press, Beijing, 1983.
[20] R.H. Wang and K.X. Guo, *Symmetry Group in Crystallography*, Science Press, Beijing, 1990.
[21] T. Hahn, *International tables for crystallography, space-group symmetry volume A*, Int. Union. Crystallogr. (2005), pp. 29–31.
[22] F. Levy, *Crystallography and Crystal Chemistry of Materials with Layered Structures*, D. Reidel, Dordrecht, 1976.
[23] G. Zhdanov, *The numerical symbol of close packing of spheres and its application in the theory of close packings*, Compt. Rend. Acad. Sci. URSS 48 (1945), pp. 39–42.
[24] A. Takeuchi and A. Inoue, *Classification of bulk metallic glasses by atomic size difference, heat of mixing and period of constituent elements and its application to characterization of the main alloying element*, Mater. Trans. 46 (2005), pp. 2817–2829.
[25] K. Kishida, K. Nagai, A. Matsumoto, A. Yasuhara, and H. Inui, *Crystal structures of highly-ordered long-period stacking-ordered phases with 18R, 14H and 10H-type stacking sequences in the Mg–Zn–Y system*, Acta Mater. 99 (2015), pp. 228–239.
[26] S.-Y. Ma, L.-M. Liu, and S.-Q. Wang, *The predominant role of Zn6Y9 cluster in the long period stacking order structures of Mg–Zn–Y alloys: A first-principles study*, J. Mater. Sci. 48 (2012), pp. 1407–1412.
[27] S.Y. Ma, L.M. Liu, and S.Q. Wang, *The clustering of Zn6Y9 and its predominant role in long period stacking order phases in Mg-Zn-Y alloys: A first-principles study*, Mater. Sci. Forum 749 (2013), pp. 569–576.
[28] Q.-Q. Jin and S.-B. Mi, *Intermetallic phases in Mg–Co–Y alloys*, J. Alloys Compd. 582 (2014), pp. 130–134.
[29] M. Egami and E. Abe, *Structure of a novel Mg-rich complex compound in Mg–Co–Y ternary alloys*, Scr. Mater. 98 (2015), pp. 64–67.